International Journal of Multiphase Flow 36 (2010) 210–220

Contents lists available at ScienceDirect

International Journal of Multiphase Flow

journal homepage: www.elsevier.com/locate/ijmulflow

Frost formation in vertical channels under natural convection

Marco Fossa [a], Giovanni Tanda [b,*]

[a] Dipartimento di Ingegneria della Produzione, Termoenergetica e Modelli Matematici (DIPTEM), Università degli Studi di Genova, via all'Opera Pia 15a, I-16145 Genova, Italy
[b] Dipartimento di Macchine, Sistemi Energetici e Trasporti (DIMSET), Università degli Studi di Genova, via Montallegro 1, I-16145 Genova, Italy

ARTICLE INFO

Article history:
Received 12 February 2009
Received in revised form 30 September 2009
Accepted 1 November 2009
Available online 10 November 2009

This paper is dedicated to the memory of Dr. Ing. Diego Garreffa, who made a significant contribution to this research before he passed away on January 6, 2007.

Keywords:
Frost
Vertical channel
Free convection
Heat/mass transfer

ABSTRACT

Processes involving heat transfer from a humid air stream to a cold plate, with simultaneous deposition of frost, are of great importance in a variety of refrigeration equipment. In this paper, frost growth on a cold, vertical plate in free convection has been experimentally investigated. The cold plate (0.095 m high, 0.282 m wide) was placed in vertical channels open at the top and bottom in order to permit the natural circulation of ambient air. The channels, rectangular in shape, were 2.395 m high and 0.36 m wide, with the depth set equal either to 20 mm, or 10 mm, or 6 mm in order to infer the influence of channel flow area on the natural convection and frost formation. The cold plate temperature and the air relative humidity were varied in the −40 to −4 °C and 31–85% range, respectively, with the air temperature held fixed at 27 °C (±1 °C). Several quantities (thickness, temperature and mass of frost, heat flux at the cold plate), were measured during the time-evolution of the process (7.5 h from the frost growth inception), and are presented as functions of the input parameters (relative humidity and cold plate temperature); in particular, the role exerted by the plate confinement on the frost growth is discussed. Data are recast in order to identify compact parameters able to correlate frost mass, thickness and density data.

1. Introduction

Frost formation occurs when humid air passes over a surface whose temperature is below the water freezing temperature. In many engineering applications, frost is undesirable. For example, a frost layer over a heat transfer surface contributes to increase the thermal resistance and thus potentially to reduce the rate of heat transfer. In channel flows, frost may also reduce the flow cross-section and result in a lower mass flow rate of air or even in a flow blockage.

The growth of frost is a complicated transient process in which both heat and mass transfer occur simultaneously. Most of the studies devoted to this topic refer to the frost formation over a cold surface exposed to a forced (channel) or a free (in open field) convective flow of humid air. In these conditions, Hayashi et al. (1977) identified three different periods in the frost formation process: (a) a crystal growth period, characterised by a one-dimensional growth of frost crystals in the direction perpendicular to the frosting surface, (b) a frost layer growth period, when the frost crystals interact with other crystals resulting in a uniform frost layer, (c) a frost layer full growth period, when the frost surface reaches 0 °C and a cyclical process of melting, freezing and deposition occurs until frost formation stops. The time for each period and the shape of frost crystals were found to strongly depend on the cooling surface temperature and the vapour concentration difference between the mean stream and the cooling surface.

The dependence of frost formation on the environmental variables and surface conditions has been studied extensively. Key parameters are the cooling surface temperature and air humidity; typically, changing the cold plate temperature mainly affects the frost thickness, while changing the relative humidity affects both frost thickness and mass rate. As for the role played by other parameters, data provided by previous studies are often not in agreement. Increasing air velocity turned out not to affect frost growth (Tokura et al., 1988), to increase it up to a critical Reynolds number (O'Neal and Tree, 1984), to increase the frost mass rate and not the thickness (Östin and Andersson, 1991), or to increase both the mass and (slightly) the thickness of frost (Lee and Ro, 2002). Similar inconsistencies were found for air temperature effects: higher air temperature (keeping the humidity ratio constant) yielded lower frost height with (Lee and Ro, 2002) and without (Sahin, 1994) an increase in mass amount, while no effect of air temperature on frost growth (for the 5–12 °C range) was found by O'Neal and Tree (1984). Moreover, cooling surface conditions (roughness, affinity with water) may affect the formation of frost nuclei as observed by Tokura et al. (1983) and Tao et al. (1993).

As clearly outlined in some review papers (O'Neal and Tree, 1985 and Mishra et al., 1997), frost formation during the forced convection of humid air has been extensively studied, while, on

* Corresponding author. Tel.: +39 010 3532881.
E-mail address: giovanni.tanda@unige.it (G. Tanda).

0301-9322/$ - see front matter © 2009 Elsevier Ltd. All rights reserved.
doi:10.1016/j.ijmultiphaseflow.2009.11.002

the other hand, only a limited number of investigations deal with mass–heat transfer during natural convection on a surface at subfreezing temperatures. This problem was tackled by Kennedy and Goodman (1974, study of frost formation on a vertical surface), Tajima et al. (1974, flat surface with different orientations), Cremers and Mehra (1982, outer side of vertical cylinders), Tokura et al. (1983, vertical surface). To the Authors' knowledge, no data are available for natural convection in channels except for their previous papers (Tanda and Fossa, 2001, 2006; Fossa and Tanda 2002a,b, 2008), despite the practical significance of this phenomenon in such devices as evaporative heat exchangers for cryogenic liquid gasification. As outlined by Tanda and Fossa (2006), the mechanism of frost formation for the free convection channel flow can be markedly different from that observed by Hayashi et al. (1977): indeed, as the free-flow area becomes too narrow due to frost growth, the buoyancy-induced air flow rate through the channel and the heat/mass transfer are markedly reduced. The combination of low surface temperatures and high air humidities typically causes the growth of a dense frost layer at the leading edge of the cold plate that obstructs a relevant part of the channel passage; the marked decrease of the convective air flow rate does not allow further significant mass deposition, and the frost surface temperature rapidly drops to the cold surface temperature. For relatively high surface temperatures and low air humidities, frost growth is fairly regular and uniform, the thickness increases slowly and rarely leads to significant obstructions of the channel passage during the time of observation.

In this paper, an experimental study of free convection frost formation inside narrow vertical channels with three different spacings is presented. Experiments, involving the measurements of local frost thickness, frost surface temperature, air-to-frost heat flux and deposited frost mass at regular time intervals, were conducted for a variety of ambient relative humidity and wall temperature conditions, while the ambient temperature was kept constant. The information obtained from experiments was used to identify the conditions for which the heat/mass transfer in the channel is markedly reduced or even suppressed as well as parameters that influence frost growth, mass deposit and density.

2. The experimental setup

A schematic view of the experimental apparatus is shown in Fig. 1. The entire apparatus and the instrumentation were placed in a large laboratory where relative humidity could be regulated over the 30–90% range at 27 ± 1 °C. The channel, made of Plexiglas and rectangular in shape, had a section of a variable depth (between 6 and 20 mm, i.e. from 0.006 to 0.02 m) and a fixed width (0.36 m) and was 2.395 m high: it was open at the top and bottom in order to permit natural circulation of ambient air. The test section, located at 1.3 m from the channel top section and at 1.0 m from the bottom section, consisted of a 0.095 m high, 0.282 m wide, cold plate and three Plexiglas walls forming a channel as deep and as wide as the entrance and exit channels. The aspect ratio of the vertical channel (ratio between the depth and the height) was a very little value (between 0.0025 and 0.00835), the aspect ratio of the cooled section of the channel (ratio between the depth S of the channel and the height H of the cold plate) was in the 0.063–0.21 range.

The cold plate was made of copper and cooled by the internal circulation of ethyl alcohol coming from a thermostatic bath. The plate was framed inside a Plexiglas wall and separated from it by 10-mm thick polystyrene strips to minimise the thermal conduction at the plate boundaries and thus prevent dew and frost formation on surfaces other than the test surface.

Each experiment was conducted with constant values of ambient air temperature and relative humidity and for a given value of the cold plate surface temperature. Namely, the temperature of the ambient air was set at a value in the range 26–28 °C, with variations in time, for each individual test, confined within 0.9 °C, while the relative humidity Rh was taken at a value between 31% and 85%, with variations in time, for each individual test, confined within 2% (in Rh units). The surface temperature T_w of the cold plate was varied in the −40 to −4 °C range, with variations in time and along the surface within ±1 °C (at the lowest T_w) and ±0.4 °C (at the highest T_w).

Before test plate cooling, the surface was covered with a thin polyethylene film so that water vapour could not condense on the test plate before the starting of the test. After the prescribed temperature of the plate was reached, the test was started by taking off the film. The standard duration of each test was 7.5 h; the monitored quantities (air, plate and frost temperatures, frost thickness, heat flux) were measured at regular time intervals (typically 30–45 min for frost thickness and air and plate temperatures, and 5–15 min for frost surface temperature and heat flux) after the test inception.

The relative humidity of the convective air flow was measured by capacitance hygrometers, carefully calibrated in the 10–95% range and positioned at the inlet and outlet of the test section. The estimated uncertainty (at the 95% confidence level, 20/1 odds) in air relative humidity was 2% (in Rh units).

The surface temperature of the cold plate was measured by five thermocouples, fitted inside small holes drilled into the wall material positioned as close as possible to the exposed surface. Numerous fine-gauge thermocouples were employed to evaluate the temperature of the air flow at the test section inlet and outlet. Additional thermocouples were located in the Plexiglas wall opposite to the cold plate (to allow the evaluation of the thermal radiation exchange) and in the material surrounding the cold plate (to allow the thermal conduction to the plate from the surrounding to be checked). Two infrared thermometers were used to measure the frost layer surface temperature at the plate midheight: the mean frost surface temperature was calculated as the average of the two individual measurements. The estimated uncertainty (at 20/1 odds) in temperature measurements was 0.1 °C for thermocouples and 0.8 °C for infrared thermometers; these sensors were characterised by the largest uncertainties in the early stage of frost formation (especially at low humidity) owing to the strong variations of the emittance of the thin frost layer.

The thickness of the frost layer was continuously monitored at the three locations A–C (see Fig. 1) corresponding to the positions of the heat flux sensors. Two alternative types of sensors were used: contact sensors and optical sensors. The contact probe consisted of a 1 mm-dia needle connected to a micrometer and moved from the Plexiglas wall (facing the cold plate) towards the frost surface until the contact was visually observed. A nylon tip needle was employed to prevent frost melting. The optical probe consisted of a co-axial glass fibre, whose tip, fitted by a lens, emits a pulsed red light. The intensity of back reflected light, proportional to the distance from the target and to the reflectivity of the target, exhibits a peak value when the distance from the target is equal to the lens focal length. In order to maximise the sensitivity of the device, the probe was mounted on a micrometer; a set of measurements (six at least) was performed at various distances from the target so as to infer, by regression analysis of individual signal values, the position of the sensor corresponding to the maximum light intensity. The measurement technique based on the contact probes is more time-consuming (great care is required to identify the contact point without damaging the growing frost layer) but relatively accurate (20/1 odds uncertainty about 0.35 mm) for every surface condition of frost; on the other hand the use of the optical probe gives rise to greater uncertainty (between 1 and 2 mm) when the frost surface is rough

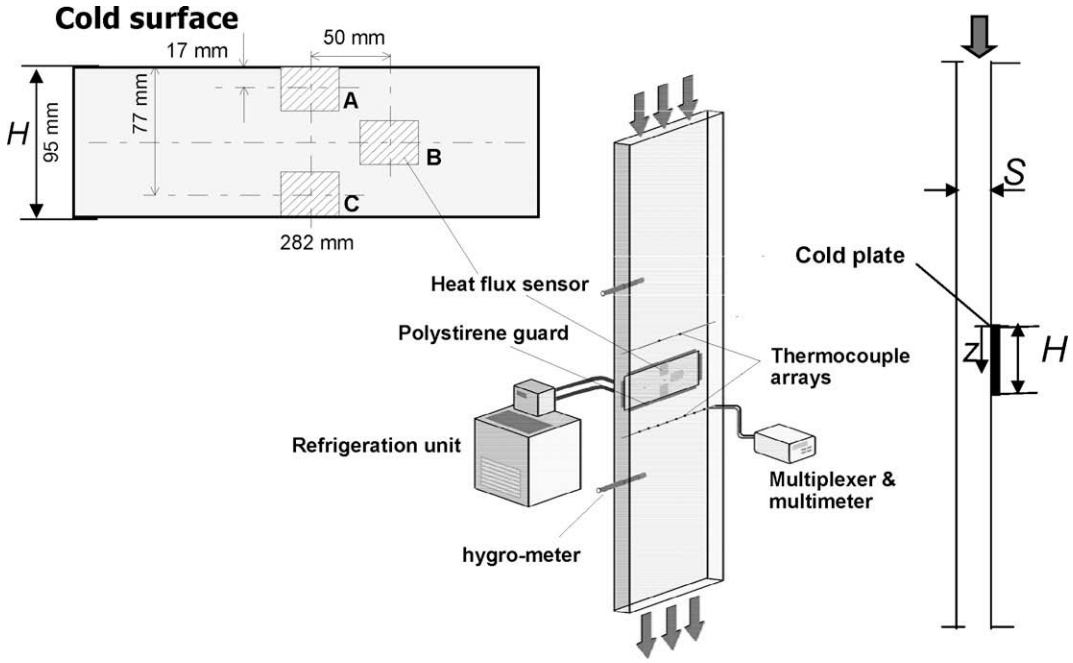

Fig. 1. Schematic layout of the vertical channel and cold plate surface.

and porous (owing to the variation of reflectance properties of the growing frost layer), whereas for compact, flat and uniform frost layers uncertainty drops to only 0.15 mm. As further validation of the described thickness measurements, additional measurements were made, by using two shielded, 0.5 mm-dia thermocouples connected to micrometers so as to travel through the cold plate (inside small holes) into the frost layer up to the frost/air interface: owing to the destructive nature of this procedure, it was applied only at the end of each test. Once established the good agreement among the different measurement procedures under standard operating conditions (presence of compact and uniform frost layer at various thicknesses), the majority of the presented thickness measurements were performed by using the contact probes, since their accuracy was found to depend only slightly on the input parameters (air temperature/humidity and cold plate temperature).

The heat flux entering the cold plate was measured by three heat flux sensors (size 1 cm^2, thickness 0.15 mm) flush-mounted on the test surface at different positions (A–C) as shown in Fig. 1. Since the thermal resistance of each heat flux sensor (about 0.002 K m^2/W) is very low as compared to the air side (or frost side) thermal resistance, their presence was expected not to locally alter the frost formation phenomenon. For the same reason, the thin lead wires were accommodated into little holes drilled across the cold plate and were not exposed to the humid air flow. The uncertainty (at 20/1 odds) in heat flux, estimated according to conductive and convective mode calibrations, was, in percentage, equal to 10%.

The deposited mass of frost was measured by a precision balance (having a resolution of 10^{-5} kg) after the frost had been scraped off the plate at the end of each test. In order to recover the temporal variation of the frost mass, additional runs were performed at different time durations and the mass was weighed at the end of each of them.

3. Results and discussion

3.1. The natural convection air flow in the channel

First, an insight of natural convection inside the channel with no frost formation has been provided by simulations with ANSYS commercial code. The channel was subdivided into 2×10^5 elements, with a typical size of $0.05 \cdot S$, S being the channel depth. The wall temperature of the cold surface of the channel was set equal to 273.15 K, the other surfaces being at 300 K, like the temperature of the inlet air.

The computed local heat transfer coefficient h along the cold surface is reported in Fig. 2. The heat transfer coefficient typically starts from a high value close to the leading edge of the surface and the decreases as the trailing edge is approached. Distributions of h for the channel depths $S = 10$ and 20 mm show a similar behaviour and both are very close (except for the entrance region) to theoretical values (Ostrach, 1952) for an isolated, isothermal vertical surface. This means that the heat/mass transfer features are very similar to those occurring along an unbounded cold vertical surface. As the channel depth is reduced to only 6 mm, the heat transfer performance is markedly decreased due to the increased friction resistances inside the channel. From an average point of

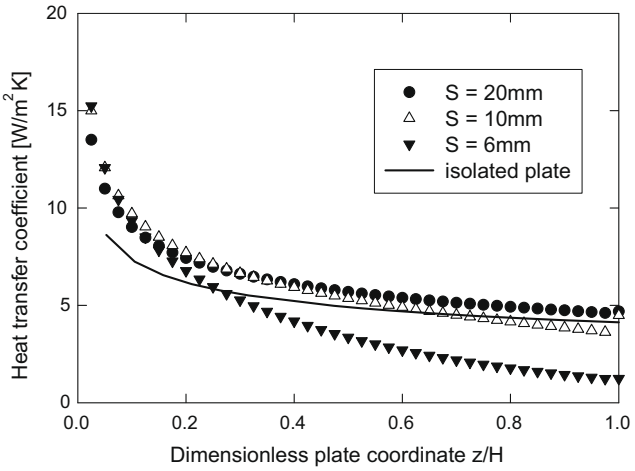

Fig. 2. Computed distributions of the heat transfer coefficient for $T_w = 273.15$ K, $T_{amb} = 300$ K, without frost formation and three different values of the channel depth S, compared with the theoretical distribution for an isolated, isothermal vertical plate (Ostrach, 1952).

view, the heat transfer coefficient is reduced by only 3% as the channel depth is contracted from 20 to 10 mm, and by 32% passing from 20 to 6 mm. As a consequence, significant alterations, relative to the deepest channel condition, are expected in free convection frost formation when the flow area is so strongly reduced: this condition may occur even when the channel depth is relatively large (10 or 20 mm) but the frost, growing onto the cold surface, becomes so thick as to induce significant flow area contractions.

3.2. Qualitative observations of frost growth

The frost formation process, studied by photographic observation, has been described by Fossa and Tanda (2008). The type of deposited frost was dependent on the operating parameters already identified by Hayashi et al. (1977), namely the cold plate temperature and the mainstream to cold plate vapour concentration difference, with the addition of the channel depth, and often can show different features along the deposition surface.

Results for frost formation inside the channel with the depth $S = 20$ mm were qualitatively similar to those observed for the free convection frost formation on surfaces without confinement. It is argued that the cold plate confinement in a channel of such depth induced only minor modifications to the frost growth process. Indeed, the growing frost layer, over the investigated time interval (7.5 h), did not significantly obstruct the flow passage, without reductions in the humid air flow rate, drawn into the channel, which feeds the mass transfer process. As observed by Hayashi et al. (1977), for high wall temperatures associated with low relative humidities the growth is characterised by small crystals at the beginning of frost formation to form, after 7.5 h, a thin, dense and uniform layer of frost. As the wall temperature is decreased and the air humidity is increased, rod-like columns of frost collapse to form a porous frost layer.

The frost growth for the channel with intermediate depth ($S = 10$ mm) has features similar to those described for the deeper channel only when the cold plate temperature is relatively high and the air humidity is low: in these conditions the frost growth characteristics in the two channels ($S = 20$ and 10 mm) are qualitatively similar (even though the frost layer grows more quickly in the deeper channel for the same operating conditions, as discussed later). For very low cold plate temperatures, a different structure is observed as a function of the relative humidity. If the air flow rate is relatively dry, a uniform and soft layer of needle-type crystals is formed; for an increased level of the air humidity, the layer quickly becomes thick and tight over the leading edge of the cold plate and remains relatively thin and soft downstream.

Frost formation in the narrowest channel ($S = 6$ mm) is strongly inhibited by the reduced air flow passage: a thick layer of frost is quickly deposited at the leading edge of the cold plate with the channel becoming partially or totally obstructed. Thus, the buoyancy-induced air tries to bypass the frost obstruction descending along the sides of the cold plate, giving rise to a frost thickness varying along the vertical and transverse directions. If the cold plate temperature is high, no frost deposition occurs in a deep region of the cold plate; if the cold plate temperature is low, in a relatively short time a thick layer of iced frost is accumulated along the top and side boundaries of the cold plate, while elsewhere the frost layer remains soft and thin owing to the shortage of incoming humid air.

3.3. Frost layer profile

The profile of the frost layer depends on several parameters. Fig. 3 schematically reports two typical frost layer outlines observed in this study: a nearly uniform frost growth that progressively develops in the direction normal to the cold plate (Fig. 3a) and a profile featured by an abrupt frost mass deposition at the leading edge followed by a thinner layer of frost (Fig. 3b). The former profile, typically recorded for free convection in an unconfined, vertical plane (Tokura et al., 1983) and cylindrical (Cremers and Mehra, 1982) surfaces, was encountered in the deepest channel ($S = 20$ mm), as already documented by Tanda and Fossa (2001), and by Fossa and Tanda (2002a, 2002b) for T_w from −13 to −4 °C and confirmed here at the lowest (−40 to −20 °C) cold plate temperatures. This regular and uniform frost growth (Fig. 3a) is not able to alter the convection inside the channel at the lowest humidity values (owing to the thin layer of deposited frost) and thus was encountered even in the case of the 10 mm deep channel. The latter profile characterises frost formation in narrow channels under special air humidity/cold plate temperature conditions. For instance, in the 10 mm deep channel, relatively high humidities combined with low cold plate temperatures promote a frost growth that is fairly uniform only during the very early stages of the transient; once the deposited frost has occupied a significant part of the free-flow area (say 50% of the available flow passage), the mass transfer still occurs at the leading edge of the cold plate (upper positions) while it ceases downstream owing to the strong reduction in the convective air flow rate, with the corresponding frost outline depicted in Fig. 3b.

In the narrowest channel ($S = 6$ mm) the blockage at the leading edge is induced in almost every operating condition and can occur within few hours from the beginning of the test. Depending on the wall temperature/air humidity conditions, the frost thickness beyond the leading edge blockage can virtually be zero or few millimetres, with a significant spanwise variation in thickness due to the air flow rate that bypasses the blockage and feeds the mass deposition coming from the small lateral gaps.

It is apparent that the performed frost thickness measurements, that were discrete and limited to three single points (A–C in Fig. 1), are of relevance only for $S = 20$ and 10 mm, with a frost growth

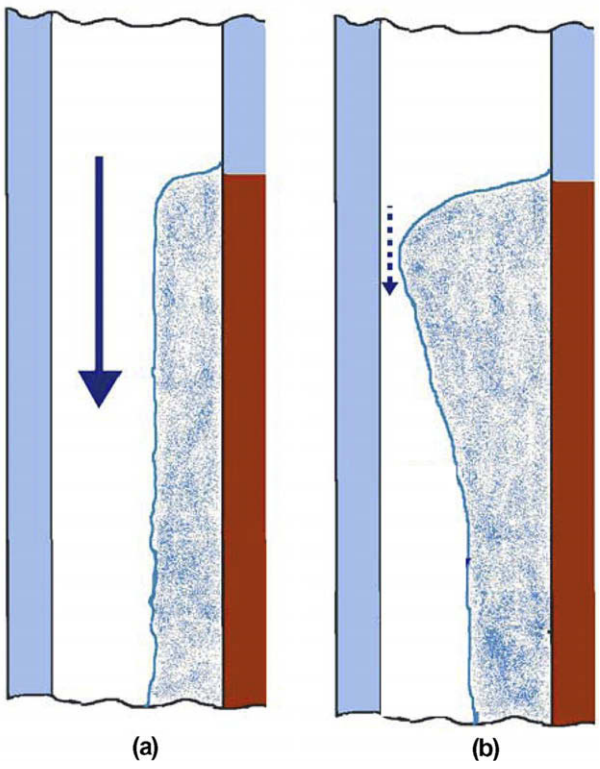

Fig. 3. Typical outlines of the frost layer. (a) Uniform frost growth. (b) Frost growth with flow obstruction at the leading edge.

with minor spanwise variations. In particular, under the frost growth depicted in Fig. 3a, i.e. with a monotonic and regular increase in the frost thickness, the latter is practically independent of plate location. This situation was typically observed for $S = 20$ mm (Fig. 4) and in certain conditions for $S = 10$ mm (Fig. 5a).

For $S = 10$ mm, the combination of high humidities and low cold plate temperatures leads to a frost thickness growth up to contact with the opposite wall, at an elevation upstream of the probe locations. As this condition occurs, the frost thickness stops increasing (first at the lowest probe location and then at the highest one) and even decreases, probably owing to densification processes, as depicted in Fig. 5b. A similar behaviour was encountered by Östin and Andersson (1991) for the forced-convective channel flow under similar (high) air humidity and (low) cold plate temperature conditions.

The frost thickness measured, for $S = 6$ mm, at the location A closer to the leading edge (Fig. 6) typically fills the entire channel depth for $T_w = -40$ °C (with a response time depending on the air humidity) while it stops before reaching the opposite wall for $T_w = -4$ °C. Thickness measurements at the downstream locations B and C were not feasible (no optical access to the tip probe due to the frost growth along the plate sides) or were virtually equal to zero (with low humidities and high wall temperatures, the cold plate was locally free of frost).

Similar considerations are reflected in the graph of Figs. 7 and 8, where the outlet air temperature T_{out} (evaluated as the average of nine independent measurements over the outside section) and the frost surface temperature T_{fs} are plotted versus time, for Rh = 70% ($T_w = -8$ °C and -30 °C) and for Rh = 31% ($T_w = -8$ °C) and two values of the channel depth ($S = 20$ and 10 mm).

At a relatively high cold plate temperature (-8 °C) and low humidity (31%), for both the channel depths ($S = 20$ and 10 mm) the thin frost layer maintains the same temperature as the cold plate, while the outlet temperature of the buoyant air flow decreases to a quasi-steady value (about 19 °C for $S = 20$ mm and 11 °C for $S = 10$ mm). When humidity is high (70%), the frost surface temperature first increases from the initial value (-8 °C) towards the freezing temperature; but for $S = 10$ mm the trend is inverted, as the frost thickness increases and the free-flow area and the heat/mass convection coefficients are progressively reduced. The air temperature downstream the cold plate quickly decreases up to a constant value (again about 20 °C) for $S = 20$ mm whereas it first decreases (to about 10 °C) and then increases slightly, for $S = 10$ mm, as a result of a decreased rate of convection heat transfer.

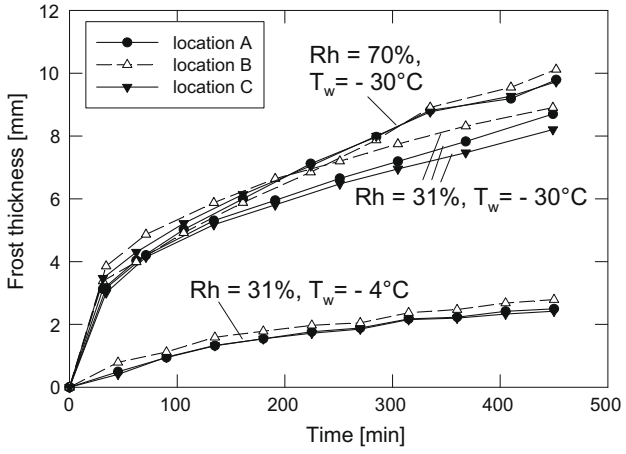

Fig. 4. Frost thickness versus time for $S = 20$ mm at different elevations (A–C) and for different values of Rh and T_w.

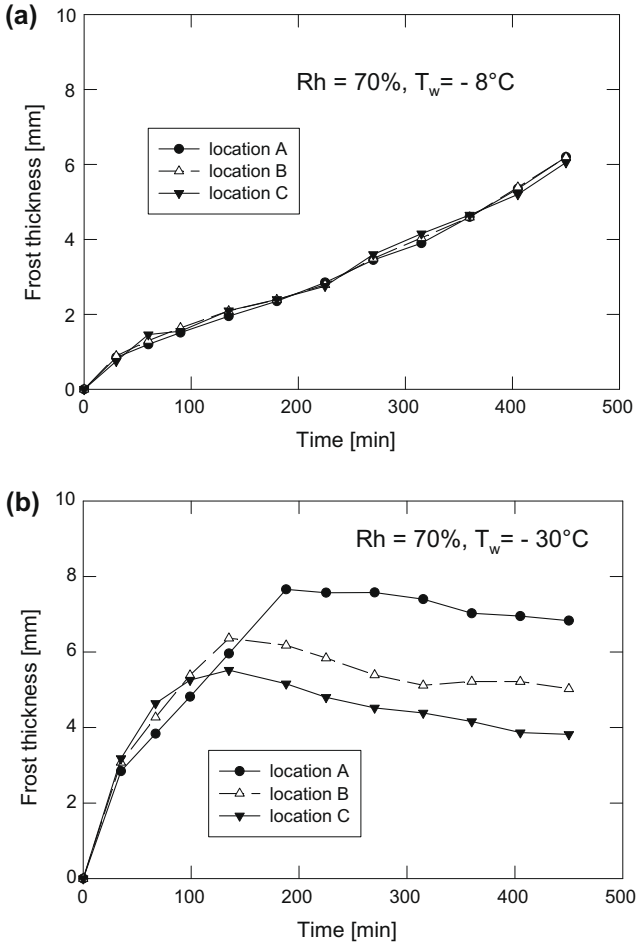

Fig. 5. Frost thickness versus time for $S = 10$ mm at different elevations (A–C): (a) Rh = 70% and $T_w = -8$ °C, (b) Rh = 70% and $T_w = -30$ °C.

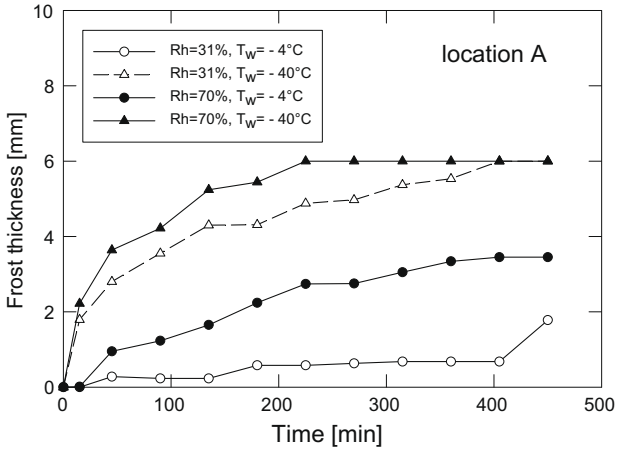

Fig. 6. Frost thickness versus time for $S = 6$ mm close to the plate leading edge (location A), for two values of Rh and at different cold plate temperatures T_w.

At the lower cold plate temperature (-30 °C) and high humidity (70%), the effect of the channel depth is more pronounced: for $S = 20$ mm the frost growth is regular and continuous in time, and the frost surface approaches a constant temperature value, close to the triple-point, in a rather short time. For $S = 10$ mm, convection is suppressed within a short transient; as a consequence, the temperature of frost surface, after the attainment of a maxi-

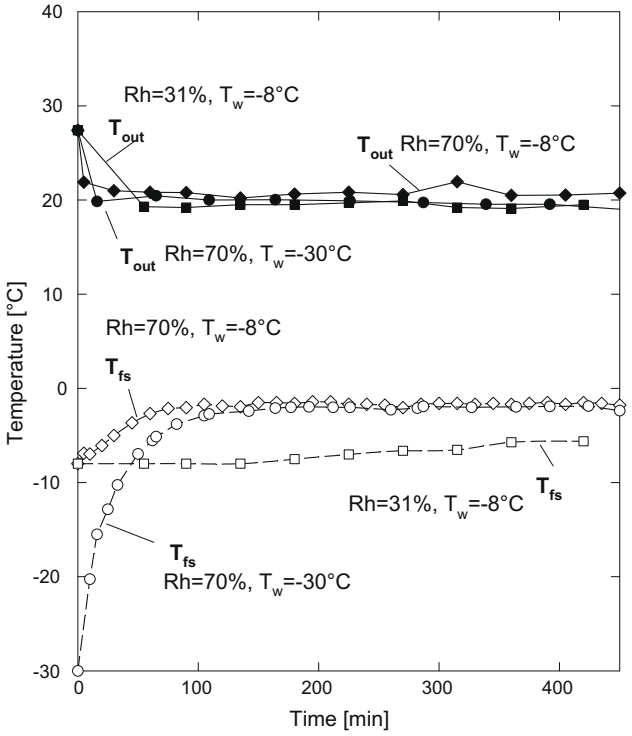

Fig. 7. Mean air temperature downstream of the cold plate (T_{out}, closed symbols) and frost surface temperature (T_{fs}, open symbols) at different Rh and T_w, for S = 20 mm.

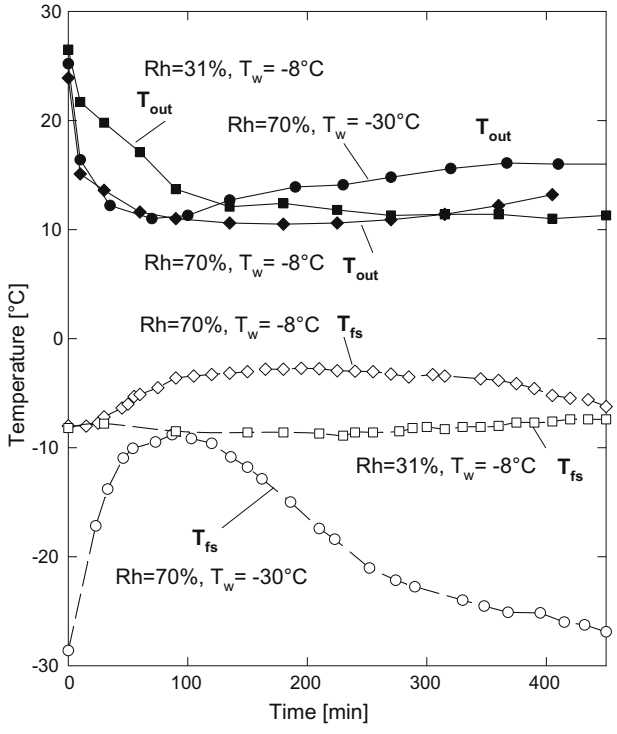

Fig. 8. Mean air temperature downstream of the cold plate (T_{out}, closed symbols) and frost surface temperature (T_{fs}, open symbols) at different Rh and T_w, for S = 10 mm.

mum value (about −9 °C), rapidly tends to the cold plate temperature, while the outlet air temperature, after a rapid decrease (to about 11 °C), progressively rises with time up to about 16 °C.

Fig. 9 shows the outlet air temperature T_{out} for the narrowest channel and two values of Rh (31% and 70%) and of T_w (−4 and −40 °C). The frost surface temperature was not reported since the infrared thermometer, located in front of the plate midheight, typically registered the same temperature as the cold plate due to the lack of frost deposit in that region. While the outlet air temperature exhibits a slight monotonic decrease with time at the higher wall temperature, it is interesting to note that, at the lower wall temperature, T_{out} first decreases in time (more rapidly for Rh = 70%) and then tends to increase as the channel becomes obstructed by the frost growth at the leading edge of the cold plate and the air flow is unable to cross the test section.

3.4. Mean frost thickness

The mean frost thickness (evaluated as the average of the three local measurements) versus time is reported in Fig 10. The figure compares the mean frost thickness profiles recorded for two values of the channel depth (S = 20 mm and 10 mm), three values of the cold plate temperature (T_w = −4, −20 and −40 °C) and three values of the air relative humidity, namely Rh = 31%, 52% and 70%.

For the lowest relative humidity (Rh = 31%, Fig. 10a), a monotonic increase of frost thickness with time is observed but the growth is faster for the deeper channel. Lower cold plate temperatures typically lead to higher frost thicknesses.

At the intermediate relative humidity level (Rh = 52%, Fig. 10b), the frost generally grows in a uniform manner (as depicted in Fig. 3a) and its average thickness still has a monotonic increase with time, except for the case of the S = 10 mm channel with low cold plate temperature, where the not regular frost growth is responsible for the attainment of a nearly constant value of the mean frost thickness.

The differences due to the two growth modes are more noticeable at the highest relative humidity (Rh = 70%, Fig. 10c). The frost thickness grows according to the scheme of Fig. 3a, for the channel relatively deep (S = 20 mm) at any cold plate temperature and for the narrower channel (S = 10 mm) with a high cold plate temperature. In the last situation, the frost grows with the same features as those of the deeper channel (S = 20 mm), with the same thickness levels and variations in time. As the channel depth and the cold plate temperature are both reduced, the mean frost thickness shows an ascending–descending profile versus time. This behaviour pertains to conditions for which the growing frost obstructs

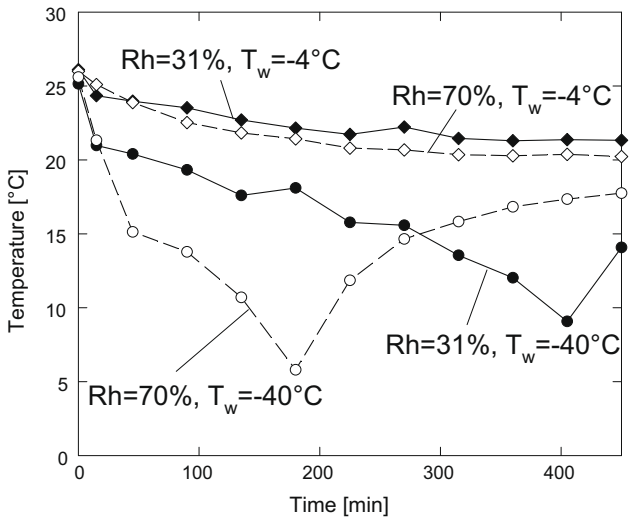

Fig. 9. Mean air temperature T_{out} downstream of the cold plate at different Rh and T_w, for S = 6 mm.

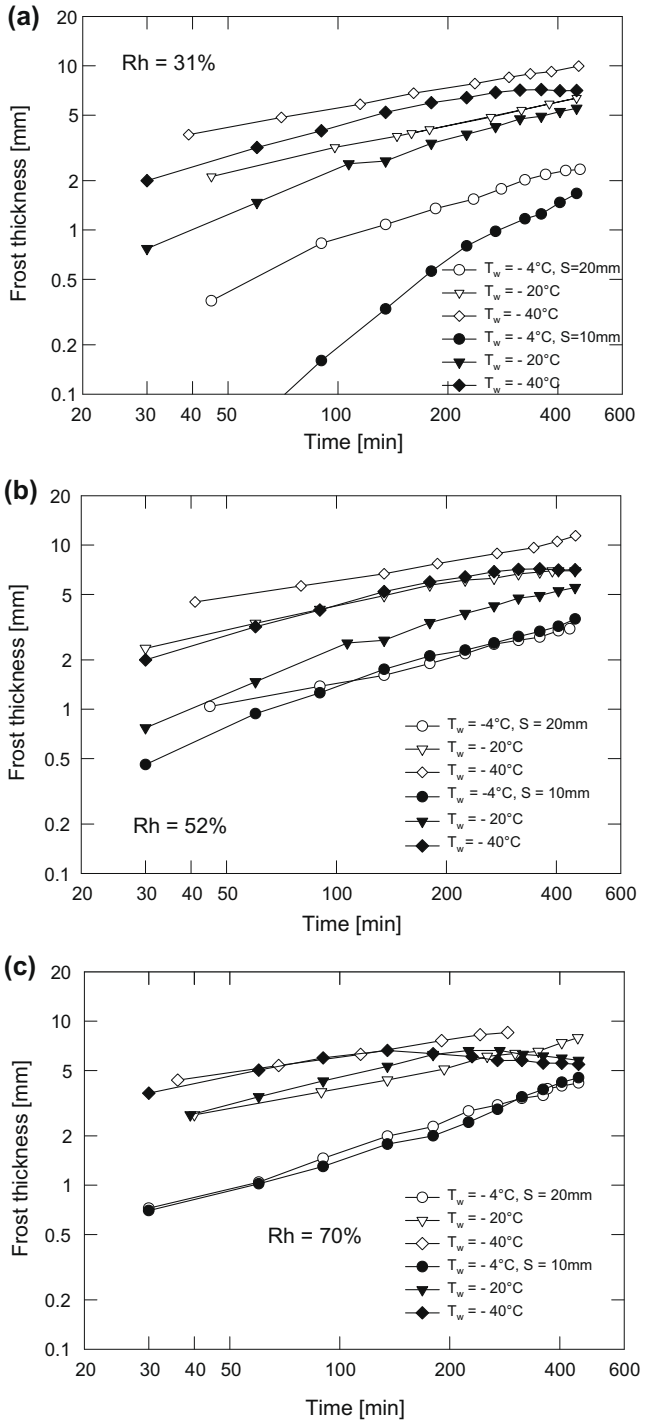

Fig. 10. Mean frost thickness versus time at different T_w, for $S = 20$ mm (open symbols) and $S = 10$ mm (closed symbols). (a) Rh = 31%, (b) 52%, and (c) 70%.

the flow passage close to the cold plate leading edge (as shown in Fig. 3b): the relative maximum of the mean thickness was about 70% of the channel depth, with the channel completely filled by frost close to the leading edge and filled at 50% close to the trailing edge. It is interesting to note that, before the attainment of the peak value, the frost growth in the $S = 10$ mm channel is again very similar to that recorded for the deeper ($S = 20$ mm) channel. As outlined by Fossa and Tanda (2008), the only exception to this trend was observed at Rh = 70% and $T_w = -8/-13$ °C with the frost layer growing faster for $S = 10$ mm and achieving, at the end of the test, a value significantly higher (by about 25–30%) than that obtained at the end of the test conducted for $S = 20$ mm and same operating conditions.

3.5. Frost surface temperature

Figs. 11 and 12 show the temperature T_{fs} of the frost surface (measured at the cold plate midheight) versus time, for different values of the cold plate temperature T_w and two different humidity Rh levels (31% and 70%), again for $S = 20$ mm and 10 mm. Measurements during the first 30 min of the frost growth (and during the whole test at Rh = 31% and $T_w = -4$ °C) were made critical by the residual reflectance of the copper cold plate affecting the signal provided by the infrared thermometer. The typical trend of T_{fs} during the frost growth on a cold surface exposed to a free convective air flow consists in a gradual increase from the initial value (T_w) towards the freezing temperature (0 °C), as observed for $S = 20$ mm (Fig. 11) and for $S = 10$ mm and low air humidity (Fig. 12a). When the convective air flow is reduced or even suppressed, the temperature of the frost surface, not efficiently heated by the buoyant air flow, stops to increase and turns towards the value of the opposite frost interface (T_w) owing to the thermal conduction through the frost layer: this trend is particularly marked at the lowest cold plate temperatures and almost over the whole range of T_w at the highest humidity for the $S = 10$ mm channel (Fig. 12b). The frost surface temperature reversal forebodes the flow blockage in the channel, that usually takes place from 1 to 2 h later. This phenomenon is the most important difference between frost growth over unconfined surfaces and frost growth in vertical channels.

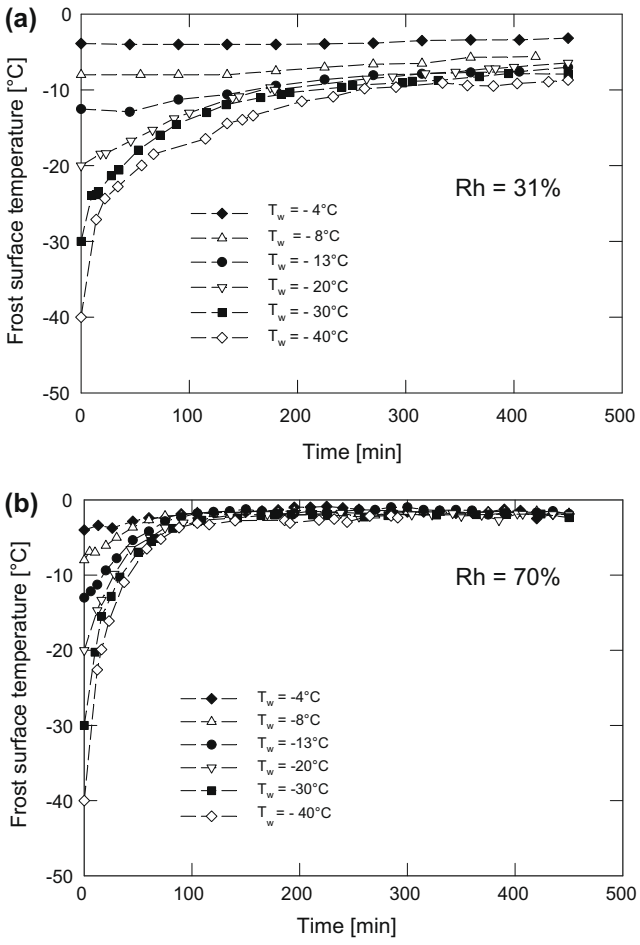

Fig. 11. Frost surface temperature T_{fs} versus time for $S = 20$ mm and different T_w values (a) Rh = 31%, (b) 70%.

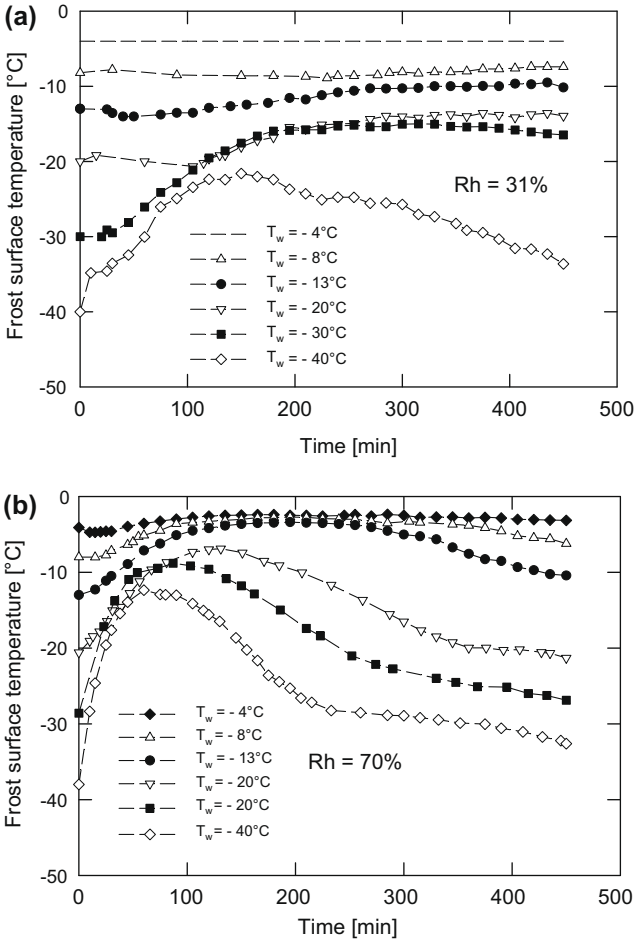

Fig. 12. Frost surface temperature T_{fs} versus time for $S = 10$ mm and different T_w values (a) Rh = 31%, (b) 70%.

Whereas, for an unbounded cold surface in the full growth frost layer regime, the frost surface temperature oscillates around zero during the cyclical process of melting and refreezing that precedes the stop of the frost deposition, in the case of the frost growth inside the channel this condition may not be attained, with the frost surface temperature never reaching the freezing temperature or abandoning that level to attain lower temperature values. As a consequence the frost formation stops because the air flow passage is completely or significantly obstructed.

3.6. Heat flux at the cold plate/frost interface

Attention is now turned to heat flux measured at the plate/frost interface for channels with depths equal to 20 and 10 mm. Since frost accumulation acts as an additional thermal resistance between the cold plate and the convective fluid, the heat transfer rate to the plate is expected to be affected by the frost growth. As described in Section 2, three plane heat flux sensors were attached to the cold plate at different elevations. Generally speaking, the sensors at locations B (midheight) and C (close to the trailing edge) gave results close to each other, while the sensor located close to the leading edge (A) recorded values with a similar trend but at higher levels, owing to the higher heat/mass transfer coefficient in that region.

Figs. 13 and 14 show heat flux measurements performed at the midheight of the plate (location B, at the same elevation as the frost surface temperature measurement). Each plot refers to heat flux variations in time at a given Rh value (namely 31% and 70%) and various cold plate temperature values. Each profile reflects the interaction between complex (and often conflicting) phenomena which act during frost formation: the spot sublimation of first crystals yielding sudden increases of heat transfer rate in the first few seconds of test (not reported in the graphs owing to the strong fluctuations in time of the signal), the thickening of the frost layer (that increases the thermal resistance of the layer and that can reduce the free flow passage), and the densification of the layer (that increases the mean density and thermal conductivity, so reducing the thermal resistance).

In general, the heat flux is strongly decreased during the first hour of test. Then, a different behaviour is displayed on the basis of the depth of the channel. For $S = 20$ mm (Fig. 13), the heat flux reaches an asymptotic value (between 300 and 600 W/m^2), typically higher as the cold plate temperature is decreased or the relative humidity is increased. For $S = 10$ mm, a similar trend is shown at the lowest Rh value (Rh = 31%, Fig. 14a): the heat flux decreases (or remains almost constant, for $T_w = -4$ and -8 °C) down to a quasi-constant value (except for $T_w = -40$ °C, for which heat flux seems to monotonically decrease), whose level is markedly reduced (typically by 25–30%) as compared to that of the larger channel. For the highest Rh value (Rh = 70%, Fig. 14b), the heat flux decreases to very low values (between 100 and 200 W/m^2) when the cold plate temperature is particularly low (from -40 to -20 °C): in these conditions the obstruction to the flow given by the deposited mass at the leading edge of the cold plate is responsible for the reduced heat/mass transfer performance at the plate

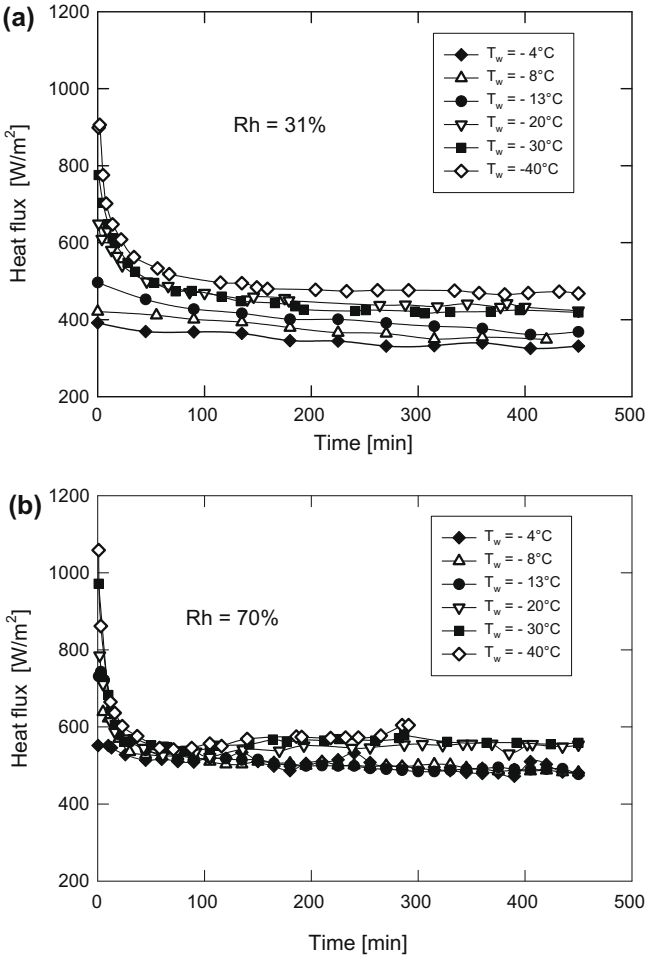

Fig. 13. Heat flux at the wall/frost interface (plate midheight, location B) versus time for $S = 20$ mm and different T_w values (a) Rh = 31%, (b) 70%.

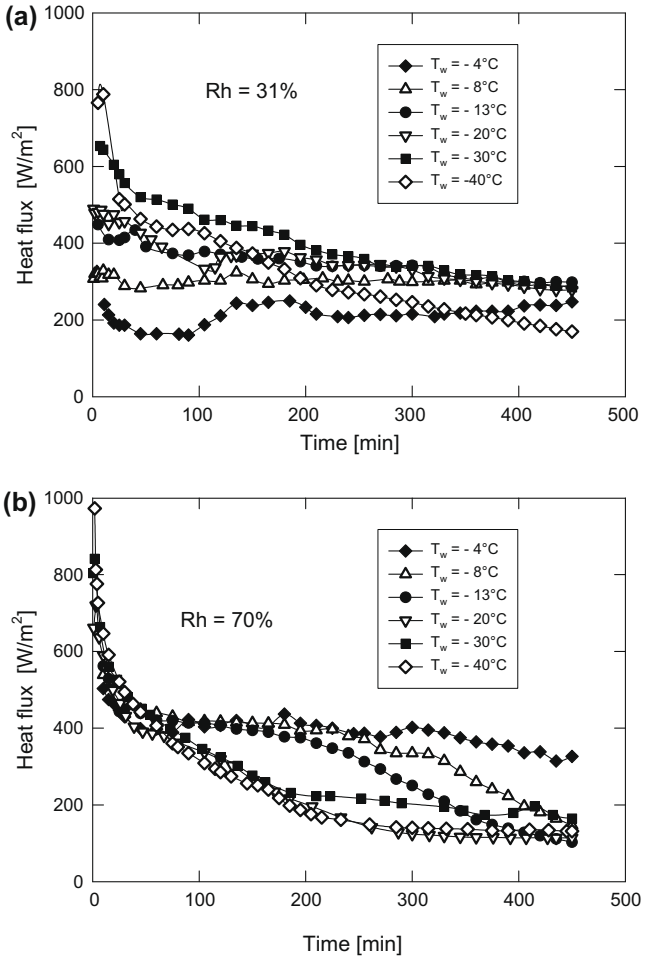

Fig. 14. Heat flux at the wall/frost interface (plate midheight, location B) versus time for $S = 10$ mm and different T_w values (a) Rh = 31%, (b) 70%.

midheight, where the fluxmeter (B) is located. At the highest cold plate temperatures (from −13 to −4 °C), heat flux profiles first attain a common value and then, after about 3-4 h (when the frost layer becomes sufficiently thick) show reductions that are more pronounced as the cold plate temperature is lowered.

3.7. Deposited mass of frost

The deposited mass (per unit area of the cold plate) during frost growth is presented in Fig. 15 for three levels of the air relative humidity (Rh = 31%, 52%, and 70%). As previously mentioned, the mass was scraped off the plate and weighed; data at intermediate time values were thus obtained by performing additional runs of different duration.

When the relative humidity is low (Fig. 15a), the deposited mass of frost in the deepest ($S = 20$ mm) and intermediate ($S = 10$ mm) channels increases almost linearly with time and the slope is mainly affected by the channel depth. Inside the narrowest channel ($S = 6$ mm), the deposition typically occurs only in the upper part of the cold plate and the amount of frost is small and increases very slowly with time.

As the relative humidity is increased (Rh = 52%, Fig. 15b and Rh = 70%, Fig. 15c), the deposited mass still shows a linear increase with time for the deepest channel ($S = 20$ mm) but the mass rate tends to increase with the relative humidity of inlet air. For the intermediate channel ($S = 10$ mm), the same trend observed for the deepest channel is noticeable at the highest cold plate temperature. When convection is weakened (owing to the flow passage

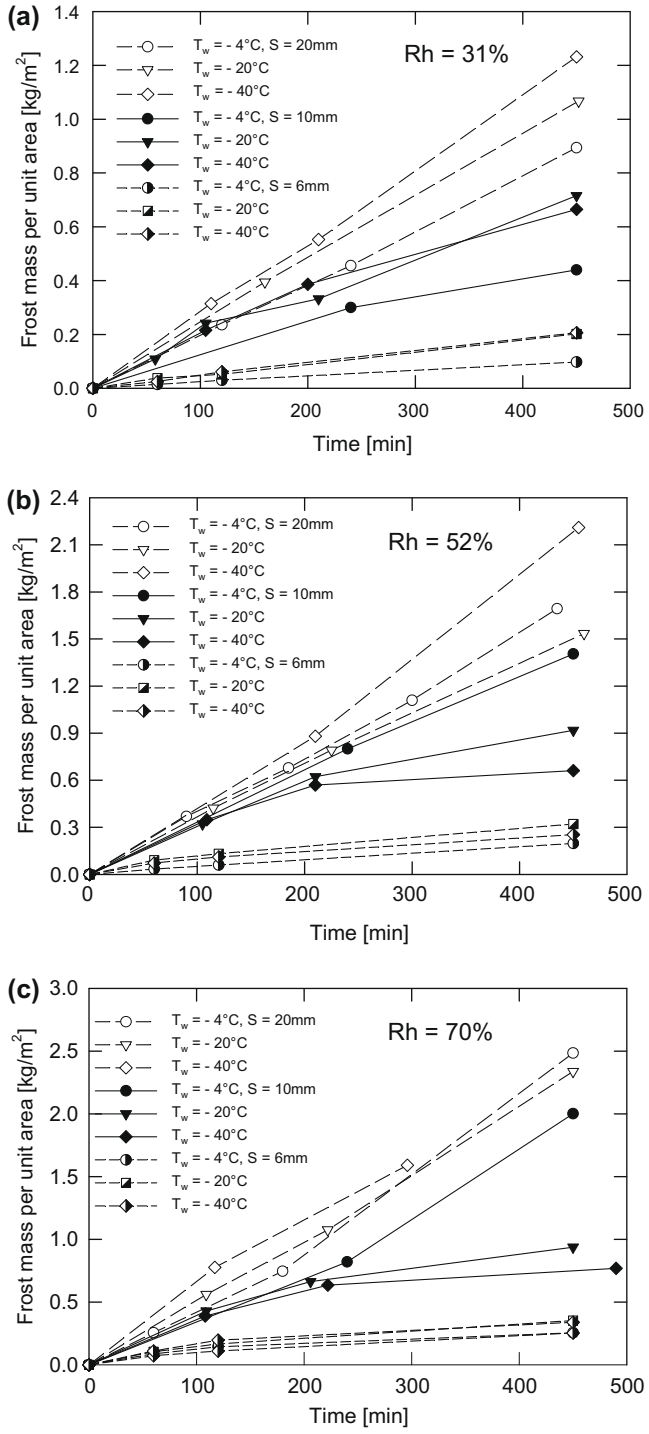

Fig. 15. Amount of deposited mass of frost versus time for different T_w values. $S = 20$ mm (open symbols), $S = 10$ mm (closed symbols), $S = 6$ mm (semi-filled symbols). (a) Rh = 31%, (b) 52%, and (c) 70%.

contraction), the mass rate is progressively reduced; this is particularly noticeable at the highest humidities and lowest cold plate temperatures. Finally, the mass deposition process in the narrowest channel ($S = 6$ mm) remains very weak, irrespective of the relative humidity levels of air.

3.8. Data reduction

Experimental results were recast in order to identify significant parameters affecting frost deposited mass, density and thickness.

Frost mass data (per unit area) m'' (in kg/m^2) have been plotted in Fig. 16 against a Mass Deposition Parameter (MDP) defined as:

$$\mathrm{MDP} = \tau[\omega_{amb} - \omega_{fs}] \quad (1)$$

where τ is the time expressed in min, ω_{amb} is the air humidity ratio, in kg$_v$/kg, measured at ambient (inlet) temperature T_{amb} and relative humidity Rh, while ω_{fs} is the air humidity ratio, in kg$_v$/kg, at frost air/interface (temperature T_{fs} and relative humidity 100%).

For the deepest channel (S = 20 mm), mass data are fitted by the following relationship:

$$m'' = 0.436 \cdot \mathrm{MDP} \quad (2)$$

with standard error of estimate 0.115 kg/m^2.

For the intermediate channel (S = 10 mm) and MDP lower than 2 min kg$_v$/kg,

$$m'' = 0.311 \cdot \mathrm{MDP} \quad (3)$$

with standard error of estimate 0.111 kg/m^2.

For highest values of MDP, Eq. (3) still holds for data obtained after a uniform growth of the frost (closed symbols) while the occurrence of the flow blockage effect at the plate leading edge leads to a slower increase in the deposited mass (open symbols), according to the following expression:

$$m'' = 0.0678 \cdot \mathrm{MDP} + 0.450 \quad (4)$$

with standard error of estimate 0.079 kg/m^2.

For the narrowest channel (S = 6 mm), the following relationship holds:

$$m'' = 0.0502 \cdot \mathrm{MDP} \quad (5)$$

with standard error of estimate 0.054 kg/m^2.

It is worth noting that the slopes of Eqs. (4) and (5) are very close to each other: this means that the frost mass grows approximately at the same velocity in the S = 6 mm deep channel and in the S = 10 mm deep channel after the flow blockage.

All the above correlations apply when the humidity ratio ω_{fs} in Eq. (1) is estimated at the temperature $T_{fs} = (273 + T_w)/2$, that represents a rough evaluation of the frost surface temperature. This is due to the fact that ω_{amb} is typically much larger than ω_{fs} so an error in the latter term does not significantly affect MDP. Eqs. (2)–(5) can thus be used to predict the deposited mass of frost as a function of environmental conditions (T_{amb}, Rh and T_w).

The mean density ρ (in kg/m^3) of the frost layer, for S = 20 and 10 mm, can be directly obtained from experiments as the ratio between the frost mass (per unit area) m'' (in kg/m^2) and the mean frost thickness δ (in mm):

$$\rho = m''/(\delta \times 10^{-3}) \quad (6)$$

A systematic analysis of all density data (including those recorded after the blockage of the channel) led to the definition of a novel parameter (termed DP, densification parameter) given by:

$$\mathrm{DP} = \tau^a \cdot (T_w/273)^b \cdot [\omega_{amb} - \omega_{fs}]^c \quad (7)$$

where τ is expressed in min, T_w in K, and ω_{amb} and ω_{fs} are the air humidity ratios, measured in kg$_v$/kg, at ambient temperature (and ambient relative humidity) and at frost surface temperature (and 100% relative humidity), respectively. The optimised values of the exponents are: a = 0.5, b = 10.22, c = 0.29. According to the above definition of DP, the mean density of frost, plotted in Fig. 17, is given by

$$\rho = a'\mathrm{DP} + b' \quad (8)$$

where a' = 109.1 for S = 20 mm and a' = 65.4 for S = 10 mm, b' being equal to 18.7, regardless of the channel depth. The standard error of estimate was 42.1 kg/m^3 for S = 20 mm and 28.9 kg/m^3 for S = 10 mm. No evaluation of ρ for S = 6 mm has been done since a reliable estimate of the mean frost thickness was not feasible.

As done for MDP, it is reasonable to evaluate DP using for T_{fs} the mean value between the cold plate temperature and the freezing temperature ($T_{fs} = (273 + T_w)/2$); again, an error in ω_{fs} has a little impact on $[\omega_{amb} - \omega_{fs}]^{0.29}$, consequently Eq. (8) can be used to evaluate the frost density as a function of ambient temperature, relative humidity and cold plate temperature.

The dependence of frost mass and density on MDP and DP respectively, has lead the authors to introduce a novel parameter (termed FTP, Frost Thickness Parameter), to correlate the mean frost thickness δ, given by the ratio between MDP and DP (Tanda and Fossa, 2006)

$$\mathrm{FTP} = \mathrm{MDP}/\mathrm{DP} = \tau^{0.5} \cdot (273/T_w)^{10.22} \cdot [\omega_{amb} - \omega_{fs}]^{0.71} \quad (9)$$

From the combination of Eqs. (2), (3), (6), (8) one obtains:

$$\delta = c'\mathrm{FTP}/(1 + c''/\mathrm{DP}) \quad (10)$$

where c' = 3.97 for S = 20 mm and 4.76 for S = 10 mm, while c'' = 0.171 for S = 20 mm and 0.286 for S = 10 mm. Eq. (10) states that in principle the mean frost thickness δ can be correlated to

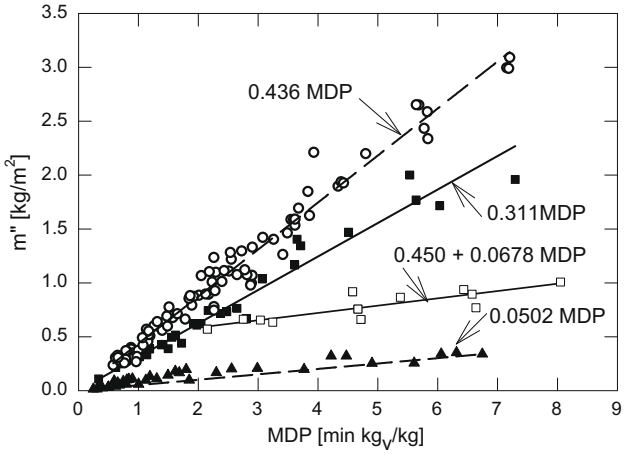

Fig. 16. Deposited frost mass correlations: mass m″ (per unit area) versus Mass Deposition Parameter (MDP). Circles: S = 20 mm, squares: S = 10 mm (filled, uniform frost growth, open, irregular frost growth with flow blockage), triangles: S = 6 mm.

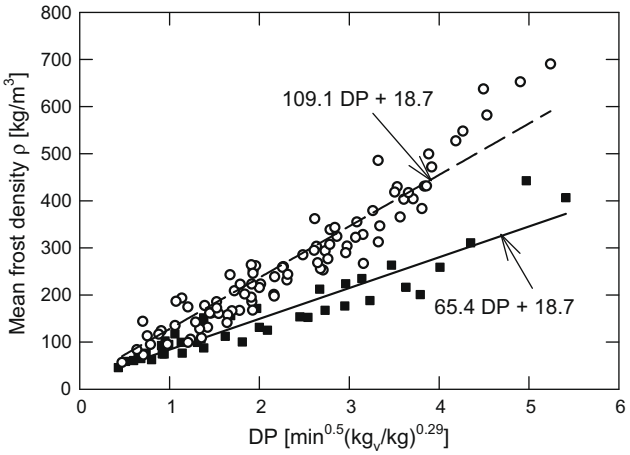

Fig. 17. Mean frost density correlations: density ρ versus Densification Parameter (DP); all experimental runs for S = 20 mm (open circles) and 10 mm (closed squares).

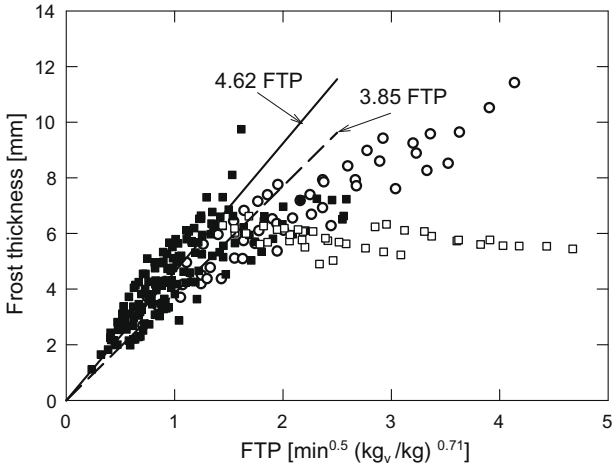

Fig. 18. Mean frost thickness correlations: thickness δ versus Frost Thickness Parameter (FTP); all experimental runs for $S = 20$ mm (open circles) and 10 mm (squares: filled, uniform frost growth, open, irregular frost growth with flow blockage).

FTP, while DP seems to affect δ only during the early stage of the frost growth (DP from 0.5 to 1). From the plot of the measured mean frost thickness versus FTP, a broad correlation between these two parameters, valid for the $S = 20$ mm and $S = 10$ mm (without flow blockage) channels, can be attempted. The frost surface temperature employed in Eq. (9) is the mean between T_w and 273 (not the measured value of T_{fs}) so as to relate FTP to input data T_{amb}, Rh and T_w. As emerges from inspection of Fig. 18, the frost thickness appears to be linearly correlated to FTP when FTP is lower than a critical value, probably controlled by the geometry of the channel, here approximately equal to 1.5. The resulting empirical relation is

$$\delta = c^* \mathrm{FTP} \tag{11}$$

where δ is in mm. The constant c^* is equal to 3.85 for $S = 20$ mm and 4.62 for $S = 10$ mm. The standard error of estimate was 0.61 mm for $S = 20$ mm and 0.76 mm for $S = 10$ mm. Assuming a constant c^* equal to 4.235 allows the estimation of δ through a single correlation

$$\delta = 4.235 \cdot \mathrm{FTP} \tag{12}$$

valid for both channels ($S = 10$ and 20 mm) with an additional error of only 10%. Since for values of FTP exceeding 1.5 the frost growth is not regular as explained in Paragraph 3.3, the prediction of δ through FTP is expected to be reliable in the FTP range from 0 to 1.5.

4. Conclusions

The frost growth process on a vertical cooling surface in free convection has been experimentally investigated. The cooling surface was placed in narrow vertical channels with different depth, open at the top and bottom in order to permit the natural circulation of ambient air. The cooling surface temperature and the air relative humidity were varied in the -40 to -4 °C and 31–85% range, respectively, while the ambient air temperature was held fixed at 27 °C (±1 °C). The depth of the channel was varied in order to infer its influence on frost formation.

In relation to studies on free convection frost growth over isolated surfaces, the presence of the confinement induced by the narrow channel was found to remarkably alter the process, especially at the lowest cold plate temperatures here explored, combined with relatively high levels of the air relative humidity. Two typical frost outlines were identified: (i) a uniform frost layer growing over the cooling surface, which progressively reduces the downmoving buoyant air flow as the free flow passage is reduced and (ii) an abrupt growth at the leading edge of the cooling surface that, in a relatively short transient, causes an obstruction to the buoyant flow with consequent interruption of frost growth and sudden reduction in heat flux from air to the cooling plate. As a consequence, except for the early stage of the process, when the frost layer is relatively thin as compared with the channel depth, predictions and relationships for frost growth and deposited mass, developed for frost growth over isolated surfaces, are expected to fail when applied to cooling surfaces inside narrow channels.

Experiments have been recast in order to envisage compact parameters useful for the prediction of frost deposited mass and density inside narrow channels. Even though the physics of the phenomenon indicates the frost surface temperature (typically unknown in practical situations) as one of the significant variables affecting the frost growth, correlations giving the time-evolution of deposited mass and mean density of frost as a function of the input data (ambient air temperature and relative humidity, cold plate temperature) have been provided. In particular, the Mass Deposition Parameter (MDP) allows the estimation of the frost deposited mass, the Densification Parameter (DP) is introduced to predict the mean frost density and the Frost Thickness Parameter (FTP) provides a general correlation for the mean frost thickness. A convenient frost surface temperature (given by the average between the cold plate and the freezing temperature) can be used in the empirical relations to overcome the difficulty of knowing this variable *a priori*.

References

Cremers, C.J., Mehra, V.K., 1982. Frost formation on vertical cylinders in free convection. ASME J. Heat Transfer 104, 3–7.
Fossa, M., Tanda, G., 2002a. Free convection frost formation on a cold plate in a vertical channel. In: Proc. 1st Int. Conf. on Heat Transfer, Fluid Dynamics and Thermodynamics, Kruger Park, SA, vol. 1, pp. 696–701.
Fossa, M., Tanda, G., 2002b. Study of the free convection frost formation on a vertical plate. Exp. Therm. Fluid Sci. 26, 661–668.
Fossa, M., Tanda, G., 2008. Qualitative observations and measurements of the free convection frost formation in vertical channels. In: Proc. 19th Int. Symposium on Transport Phenomena, Reykjavik, Iceland.
Hayashi, Y., Aoki, A., Adachi, S., Hori, K., 1977. Study of frost properties correlating with frost formation types. ASME J. Heat Transfer 99, 239–245.
Kennedy, L.A., Goodman, J., 1974. Free convection heat and mass transfer under conditions of frost deposition. Int. J. Heat Mass Transfer 17, 477–484.
Lee, Y.B., Ro, S.T., 2002. Frost formation on a vertical plate in simultaneously developing flow. Exp. Therm. Fluid Sci. 26, 939–945.
Mishra, S., Gidwani, A., Ohadi, M.M., Dessiatoun, S.V, 1997. An overview of basic models of frost formation phenomenon and recent progress on the use of an electric field in suppressing or promoting frost. In: Proc. AIChE Symp. Series Heat Transfer, Baltimore, USA, vol. 93, pp. 197–210.
O'Neal, D.L., Tree, D.R., 1984. Measurement of frost growth and density in a parallel plate geometry. ASHRAE Transactions 90, 278–290.
O'Neal, D.L., Tree, D.R., 1985. A review of frost formation in simple geometries. ASHRAE Transactions 91, 267–281.
Östin, R., Andersson, S., 1991. Frost growth parameters in a forced air stream. Int. J. Heat Mass Transfer 34, 1009–1017.
Ostrach, S., 1952. An analysis of laminar free-convection flow and heat transfer about a flat plate parallel to the direction of the generating body force. Report NACA TN 2635.
Sahin, A.Z., 1994. An experimental study on the initiation and growth of frost formation on a horizontal plate. Exp. Heat Transfer 7, 101–119.
Tajima, O., Naito, E., Nakashima, K., Yamamoto, H., 1974. Frost formation on air coolers, part 3: natural convection for a cooled vertical plate. Heat Transfer Jpn. Res. 3, 55–66.
Tanda, G., Fossa, M., 2001. An experimental study of the frost formation on a cold surface in free convective flow. In: Proc.5th World Conf. on Exp. Heat Transfer, Fluid Mech. and Thermodynamics, Thessaloniki, GR, vol. 1, pp. 693–697.
Tanda, G., Fossa, M., 2006. Free convection frost growth in a narrow vertical channel. Int. J. Heat Mass Transfer 49, 1946–1957.
Tao, Y.X., Besant, R.W., Mao, Y., 1993. Characteristics of frost growth on a flat plate during the early growth period. ASHRAE Transactions 99, 746–753.
Tokura, I., Saito, H., Kishinami, K., 1983. Study on properties and growth rate of frost layers on cold surfaces. ASME J. Heat Transfer 105, 895–901.
Tokura, I., Saito, H., Kishinami, K., 1988. Prediction of growth rate and density of frost layer developing under forced convection. Waerme und Stoff 22, 285–290.